

PAPER • OPEN ACCESS

Solid-state nuclear magnetic resonance study of setting mechanism of β -tricalcium phosphate—inositol phosphate composite cements

Recent citations

- [Bio-responsive materials for tissue regeneration](#)
Zuyong Wang *et al*

To cite this article: Toshiisa Konishi *et al* 2019 *J. Phys. Mater.* **2** 034007

View the [article online](#) for updates and enhancements.



PAPER

OPEN ACCESS

RECEIVED
16 January 2019REVISED
5 April 2019ACCEPTED FOR PUBLICATION
10 April 2019PUBLISHED
3 June 2019

Original content from this work may be used under the terms of the [Creative Commons Attribution 3.0 licence](#).

Any further distribution of this work must maintain attribution to the author(s) and the title of the work, journal citation and DOI.



Solid-state nuclear magnetic resonance study of setting mechanism of β -tricalcium phosphate–inositol phosphate composite cements

Toshiisa Konishi^{1,2,3} , Kohei Yamashita¹, Kohei Nagata⁴, Poon Nian Lim² , Eng San Thian² and Mamoru Aizawa⁵

¹ Graduate School of Natural Science and Technology, Okayama University, 3-1-1 Tsushima-naka, Kita-ku, Okayama 700-8530, Japan

² Department of Mechanical Engineering, National University of Singapore, 9 Engineering Drive 1, Singapore 117576, Singapore

³ Tokyo Metropolitan Industrial Technology Research Institute, 2-4-10 Aomi, Koto-ku, Tokyo 135-0064, Japan

⁴ Organization for the Strategic Coordination of Research and Intellectual Property, Meiji University, 1-1-1 Higashimita, Tama-ku, Kawasaki 214-8571, Japan

⁵ Department of Applied Chemistry, School of Science and Technology, Meiji University, 1-1-1 Higashimita, Tama-ku, Kawasaki 214-8571, Japan

E-mail: konishi.toshiisa@iri-tokyo.jp

Keywords: β -tricalcium phosphate, calcium-phosphate cement, inositol phosphate, solid-state NMR, setting mechanism

Supplementary material for this article is available [online](#)

Abstract

Solid-state nuclear magnetic resonance (NMR) spectroscopy is a technique, which can be used to provide insight into the chemical structure of non-crystalline and crystalline materials. Hence, the present study aimed to elucidate the setting mechanism of CPC, which was fabricated using β -tricalcium phosphate (β -TCP)—inositol phosphate (IP6) composite powder using NMR. In addition, the effect of IP6 on the local chemical structure of the β -TCP-IP6 composite powder and its hardened cement would also be investigated. The $^1\text{H} \rightarrow ^{31}\text{P}$ heteronuclear correlation NMR spectrum revealed that an amorphous hydrated layer, along with small amount of hydroxyapatite (HA) was formed on the surface of β -TCP during the ball-milling process. Results demonstrated that the IP6 in the hydrated layer on the surface of β -TCP inhibited the formation of HA. Moreover, the setting reaction of the cement was mainly triggered by the dissolution of the amorphous hydrated layer on β -TCP surface, and subsequent precipitation, followed by the inter-entanglement between the HA crystals on the β -TCP.

1. Introduction

Bioresorbable β -tricalcium phosphate (β - $\text{Ca}_3(\text{PO}_4)_2$; β -TCP) has been used for bone grafting and calcium-phosphate cement (CPC) component. Moldable or injectable CPC is capable of forming desirable shapes during surgical operation, and has therefore received considerable attention [1].

We have developed a bioresorbable β -TCP cement using inositol phosphate ($\text{C}_6\text{H}_6(\text{OPO}_3\text{H}_2)_6$; IP6) as a chelating agent, and demonstrated that the β -TCP cement had favorable biocompatibility *in vitro* and bioresorbability *in vivo* [2]. The β -TCP-IP6 composite powder was prepared by ball-milling as-prepared β -TCP powder in IP6 solution, and thereafter β -TCP cement was formed by mixing the composite powder with 2.5 mass% sodium hydrogen phosphate (Na_2HPO_4) mixing solution. Our previous study also demonstrated that the cement formed small amount of hydroxyapatite (HA) phase and its entanglement which were involved in the setting of the cement [2]. However, the chemical state of IP6 in the cement powder, the effect of IP6 on the setting of the cement, and the setting mechanism of the cement remain unknown, and have not been fully clarified.

X-ray diffraction (XRD) is a general method that is used to identify the crystal structure of a material. However, XRD does not allow the characterization of non-crystalline phase, as a result structural information on such phase cannot be obtained. Meanwhile, solid-state nuclear magnetic resonance (NMR) spectroscopy is a technique, which can be used to provide insight into the chemical structure of both non-crystalline and

crystalline materials. Thus, NMR might be a useful for understanding the local chemical structure and setting reaction of cement by characterizing the amorphous phase that was produced during the ball-milling process. At present, there are only a few NMR studies reported on local chemical structure of the cement [3, 4]. Hence, this study aimed to provide detailed investigation on local chemical structure of cement powder and fabricated cement using the solid-state NMR spectroscopy. In addition, the chemical state of IP6 in the cement powder and the effect of IP6 on the setting reaction of the cement would also be investigated to elucidate the setting mechanism of the cement.

2. Theoretical and experimental methods

2.1. Preparation of β -TCP-IP6 composite powders and cements

The β -TCP-IP6 composites powders were prepared according to our previous report [2]. Briefly, 10 g of commercially available β -TCP powder (β -TCP-100, Taihei Chemical Industrial Co. Ltd, Japan) were ground using a planetary mill for 3 h at a rotation rate of 300 rpm in a ZrO_2 pot using 180 g ZrO_2 beads with 2 mm diameter in 3000 ppm IP6 solution or ultrapure water (0 ppm IP6 solution). After ball-milling, the slurry mixture was filtered, washed with ultrapure water, and freeze-dried for 24 h. The samples were denoted as follows: β -TCP powder ball-milled in 3000 ppm IP6 was denoted as '(3000)-P'. The (0)-P and (3000)-P had a median size of $2.7 \pm 0.1 \mu\text{m}$ and $1.9 \pm 0.1 \mu\text{m}$, respectively [2]. A concentration of 3000 ppm IP6 was selected in this study because our previous report demonstrated that the β -TCP cement fabricated with 3000 ppm IP6 had superior mechanical property (14 MPa) together with *in vivo* osteoconductivity [2]. To obtain a calcium phytate (Ca-IP6) as a reference material, 10 ml of 1 mol l^{-1} calcium chloride were poured into 100 ml of 10 000 ppm solution (pH 7.3) with stirring. The precipitate was centrifuged at 6000 rpm for 5 min, rinsed with ultrapure water, and centrifuged again. This process was repeated thrice, and the precipitate was dried at 105°C for 24 h. In order to examine the chemical stability of (0)-P and (3000)-P, both the powders were kept at 37°C at 100% relative humidity for 0, 1, 2, 3, 4, 5, and 6 months.

Cement paste was prepared by mixing (0)-P or (3000)-P and 2.5 mass% of Na_2HPO_4 solution at a powder/liquid (P/L) ratio of $1/0.7 \text{ [g cm}^{-3}\text{]}$. The resulting cement paste was packed into a cylindrical mold (8 mm in diameter, 10 mm in height), hardened at 37°C at 100% relative humidity for 24 h, and ground in an agate mortar with a pestle. The powdered cement was used for its characterization except for scanning electron microscopy (SEM). The samples were denoted as follows: cement fabricated with (3000)-P was denoted as '(3000)-C'. In order to examine the phase conversion of pure β -TCP powder to HA with Na_2HPO_4 , β -TCP-100 powder was mixed with 2.5 mass% of Na_2HPO_4 at $P/L=1/0.7$, and the prepared cement was kept at 100% relative humidity up to 30 d.

2.2. Characterization of β -TCP-IP6 composite powders and cements

Crystalline phase was measured using an x-ray diffractometer (XRD; X'pert PRO, PANalytical, the Netherlands), equipped with CuK_α radiation source, $k = 1.5418 \text{ \AA}$, 45 kV, 40 mA. The crystalline phase was identified with respect to the JCPDS-ICDD PDF reference patterns for β -TCP (09-0169) and HA (09-0432). Fourier-transform infrared (FT-IR) spectra were measured by a KBr method using a FT-IR spectrometer (NEXUS 470, Thermo Nicolet, USA) with a resolution of 4 cm^{-1} . The surface microstructure inside the (3000)-C was observed by SEM (JSM-6390LA, JEOL, Japan) at an accelerating voltage of 10 kV after sputter-coating with Pt.

Local chemical structure around the hydrogen, carbon, and phosphorus atoms was analyzed by a solid-state ^1H , ^{13}C , and ^{31}P magic-angle spinning NMR (MAS NMR) spectroscopy, using an Agilent DD2 500 MHz NMR spectrometer (Agilent Technologies, Inc., USA), equipped with a cross-polarization (CP)-MAS probe. The MAS spinning rates were 12 or 15 kHz, and a zirconia sample tube with 3.2 mm diameter was used. The ^{31}P MAS-dipolar decoupling (DD) NMR spectra were recorded at 11.7 T and 202.31 MHz with $1.4 \mu\text{s} (\pi/4)$ pulse and a recycle delay (d_1) of 90, 120, or 1800 s, where the signals for 8–96 pulses were accumulated. Ammonium dihydrogenphosphate ($\delta = 1.0 \text{ ppm}$ with respect to phosphoric acid (85%): $\delta = 0 \text{ ppm}$) was used as the secondary external reference. The ^{31}P MAS-high power decoupling (HD) NMR spectra at 11.7 T and 202.31 MHz were recorded with $1.4 \mu\text{s} (\pi/4)$ pulse, $d_1 = 1$ or 120 s, where the signals for 8 pulses were accumulated. The $^1\text{H} \rightarrow ^{13}\text{C}$ CP-MAS NMR spectra were recorded at 11.7 T and 125.674 MHz with $2.3 \mu\text{s} (\pi/2)$ pulse, $d_1 = 5 \text{ s}$, and a contact time of 1 ms, where the signals for 5440–38042 pulses were accumulated. Adamantane ($\text{C}_{10}\text{H}_{16}$; $\delta = 38.52 \text{ ppm}$ with respect to tetramethylsilane: $\delta = 0 \text{ ppm}$) was used as the secondary external reference. The $^1\text{H} \rightarrow ^{31}\text{P}$ CP-MAS NMR spectra were recorded at 11.7 T and 202.31 MHz with $2.3 \mu\text{s} (\pi/2)$ pulse, $d_1 = 1 \text{ s}$, and a contact time of 1800 μs , where the signals for 1000 pulses were accumulated. Two-dimensional (2D) $^1\text{H} \rightarrow ^{31}\text{P}$ heteronuclear correlation (HETCOR) NMR spectra were

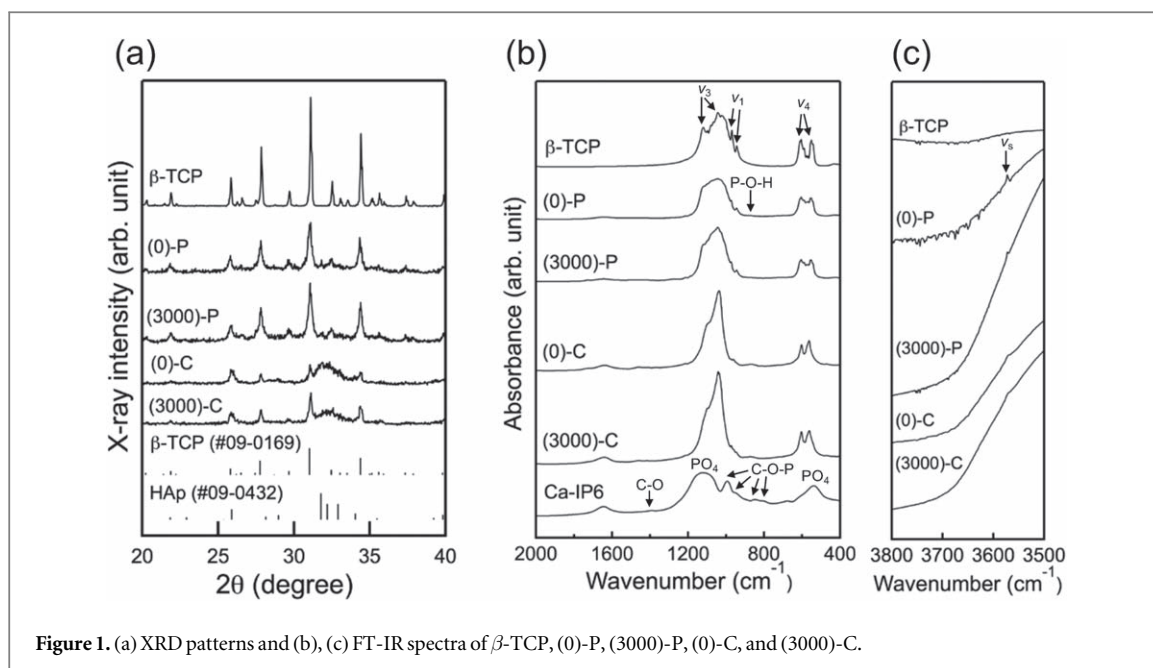


Figure 1. (a) XRD patterns and (b), (c) FT-IR spectra of β -TCP, (0)-P, (3000)-P, (0)-C, and (3000)-C.

Table 1. HA (2 1 1)/ β -TCP (0 2 10) ratio in x-ray diffraction intensity and FWHM of (0 2 10) in β -TCP, (0)-P, (3000)-P, (0)-C, and (3000)-C.

Sample	HA (2 1 1)/ β -TCP (0	FWHM of β -TCP (0
	2 10)	2 10)
β -TCP	0	0.09
(0)-P	0.17	0.23
(3000)-P	0.10	0.24
(0)-C	1.10	0.16
(3000)-C	0.45	0.15

recorded using CP with a contact time of 1 ms, $d1 = 5$ s, and 59–142 scans per t_1 increments; 128 t_1 slices were acquired, with the rotor spinning frequency controlled to be 15 kHz.

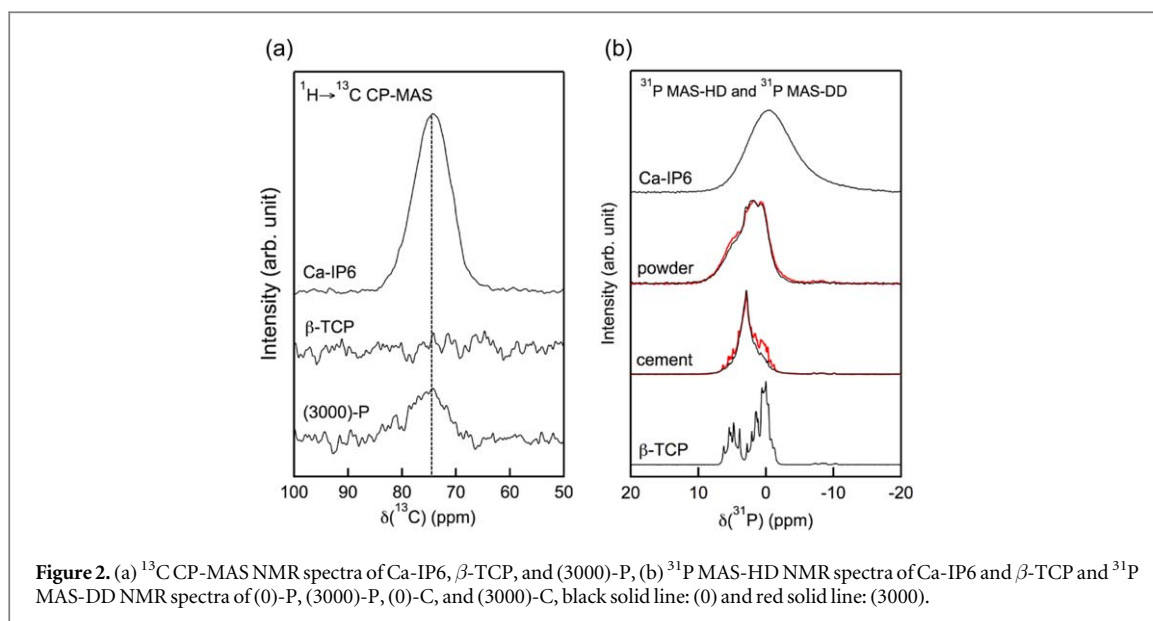
3. Results and discussion

Diffraction peaks, which corresponded to β -TCP (09-0169) were detected in all the XRD patterns (figure 1(a)). The small diffraction peaks that corresponded to HA (09-0432) at around 31° were observed in (0)-P and (3000)-P, while more intense HA diffraction peaks were observed in (0)-C and (3000)-C. The ratios of the diffraction intensity of HA and β -TCP for (0)-P were slightly higher than (3000)-P (table 1), thereby suggesting slight conversion ratio of (3000)-P from β -TCP to the HA than (0)-P. In contrast, (0)-C; 1.10, were considerably higher than (3000)-C; 0.45, which suggested considerable lower conversion ratio of (3000)-P than (0)-C. The FWHMs of (0)-P and (3000)-P were higher than that of β -TCP, which showed lower crystallinity of (0)-P and (3000)-P as compared to β -TCP that were caused by ball-milling.

The FT-IR spectra showed that the phosphate peaks corresponded to ν_1 , ν_3 , and ν_4 in all the spectra except for Ca-IP6 (figure 1(b)) [5]. In addition, the hydrogen phosphate group (~ 875 cm^{-1}) and hydroxyl group (ν_s , ~ 3575 cm^{-1}) were observed in (0)-P, (3000)-P, (0)-C, and (3000)-C (figure 1(c)). The FT-IR spectrum of Ca-IP6 exhibited C–O–P vibrations ($\sim 801, 852, 930, 994$ cm^{-1}) [6], PO_4 groups ($\sim 542, 1130$ cm^{-1}) [7], and C–O stretching vibration (~ 1397 cm^{-1}) [7], whereas, no IP6 related peak was observed in (0)-P, (3000)-P, (0)-C, and (3000)-C.

The surface microstructures of the 3000-(C) as observed using SEM showed tightly packed cement particles (figure S1(a) in the supplementary data, available online at stacks.iop.org/JPMATER/2/034007/mmedia), along with entangled rod-like crystals, were likely HA precipitates (figure S1(b)). In addition, relatively large grains which were presumably to be unreacted β -TCP grains (white arrowheads), were observed.

The $^1\text{H} \rightarrow ^{13}\text{C}$ CP-MAS NMR spectrum of Ca-IP6 demonstrated a peak at around 75 ppm (figure 2(a)). The peak was also observed in (3000)-P, but not in β -TCP, which implied that IP6 molecules existed in (3000)-P. The



^{31}P MAS-HD and MAS-DD NMR spectra in figure 2(b) showed no spectrum difference in (0)-P and (3000)-P with and without IP6. The intense peak (2.8 ppm) corresponding to HA [8] was detected in (0)-C and (3000)-C, while intense peaks corresponding to β -TCP were observed in (3000)-C than (0)-C. From the peak separation of the spectra, the remaining β -TCP phase was 48.8% for (0)-C and 61.3% for (3000)-C. Previous study [2] demonstrated that the remaining β -TCP contents of the hardened cement calculated by x-ray intensities were 20.6% for (0)-C ($P/L=1/0.8$) and 75.1% for (3000)-C ($P/L=1/0.7$). The discrepancy in the amount of the remaining β -TCP phase was probably due to a different calculation method and/or calculation without considering the background in XRD patterns. Nevertheless, the amount of β -TCP phase remained in (0)-C and (3000)-C was different in both studies.

The 2D $^1\text{H}\rightarrow^{31}\text{P}$ HETCOR NMR spectra for (a) (0)-P and (b) (3000)-P are shown in figure 3. The slice spectrum peak of (0)-P taken at 0 ppm in the ^1H dimension, which was attributed to protons of OH^- ions in the HA lattice [9], had a correlation with the broad ^{31}P peak at 3.0 ppm allocated to PO_4^{3-} ions [10] (figure 3(c)). A correlation between the ^1H peak at 5.2 ppm attributed to protons of the adsorbed H_2O molecules [9] and the broad ^{31}P peak at 2.6 ppm attributed to PO_4^{3-} ions in HA lattice [9] was observed. As the ^{31}P peak position of 2.6 ppm was close to 3.0 ppm of HA, this result indicated that amorphous hydrated layers were presented on the HA surface. The ^1H peak at 12.1 ppm was attributed to the acidic protons in hydrogen phosphate (HPO_4^{2-}) ions in octacalcium phosphate (OCP) [11]. This ^1H peak (12.1 ppm) correlated with the broad ^{31}P peaks at -0.1 ppm that was assignable to protons of HPO_4^{2-} ion in OCP [11], at 1.7 ppm attributed to HPO_4^{2-} ions of dicalcium phosphate dehydrate (DCPD) [10], and at 1.9 ppm (unassignable).

The slice spectra taken in ^{31}P dimension in figure 3(a) are shown in figure 3(d). The ^{31}P peak at 0 ppm corresponded to HPO_4^{2-} ion in OCP [11]. This ^{31}P peak (0 ppm) had correlations with the ^1H peaks at 5.3 ppm corresponding to the protons of adsorbed H_2O molecules [9], at 10.2 ppm attributed to the protons of HPO_4^{2-} ion in DCPD [10], at 12.1 ppm attributed to the protons of HPO_4^{2-} ion in OCP [11], and at 15.7 ppm corresponding to the protons with strong hydrogen bonds [10, 11]. The correlations of the ^{31}P peaks at 1.4 and 2.8 ppm allocated to HPO_4^{2-} ions in DCPD [10] and PO_4^{3-} ions in the HA lattice [9], respectively, were the same as the correlations of ^{31}P peak at 0 ppm. However, the strong correlation between the ^{31}P peaks at 1.4 and 2.8 ppm and the ^1H peak at 0 ppm that was assignable to protons of OH^- ions in the HA lattice [9] was observed.

The slice spectra of (3000)-P had the same correlations at almost the same positions, as compared to (0)-P (figures 3(e) and (f)). In addition, the slice spectrum taken at -1.0 ppm in ^{31}P dimension in figure 3(b) had the same correlations with the slice spectrum taken at 0.3 ppm in ^{31}P dimension.

In the $^1\text{H}\rightarrow^{31}\text{P}$ HETCOR NMR spectra of (0)-P and (3000)-P (figure 3), the ^1H peaks (10–16 ppm) that were attributed to the acidic proton of HPO_4^{2-} ions [9, 11] correlating with the broad ^{31}P peaks (1.4–2.0 ppm) had a similar shape and peak position with the $^1\text{H}\rightarrow^{31}\text{P}$ CP-MAS NMR spectrum of β -TCP. Thus, these correlations were considered to be the amorphous hydrated layer on the β -TCP surface. In addition, as compared to the intensity of the $^1\text{H}\rightarrow^{31}\text{P}$ correlation peaks corresponding to the HA and the amorphous hydrated layer (figure 3), (3000)-P had higher ratio of amorphous hydrated layer than (0)-P. The result implied that the IP6 might have inhibited the conversion of β -TCP to amorphous hydrated layer on the β -TCP, and subsequent formation of HA. Thus, (0)-P and (3000)-P had almost identical chemical structure but with a different ratio of HA and amorphous hydrated layer.

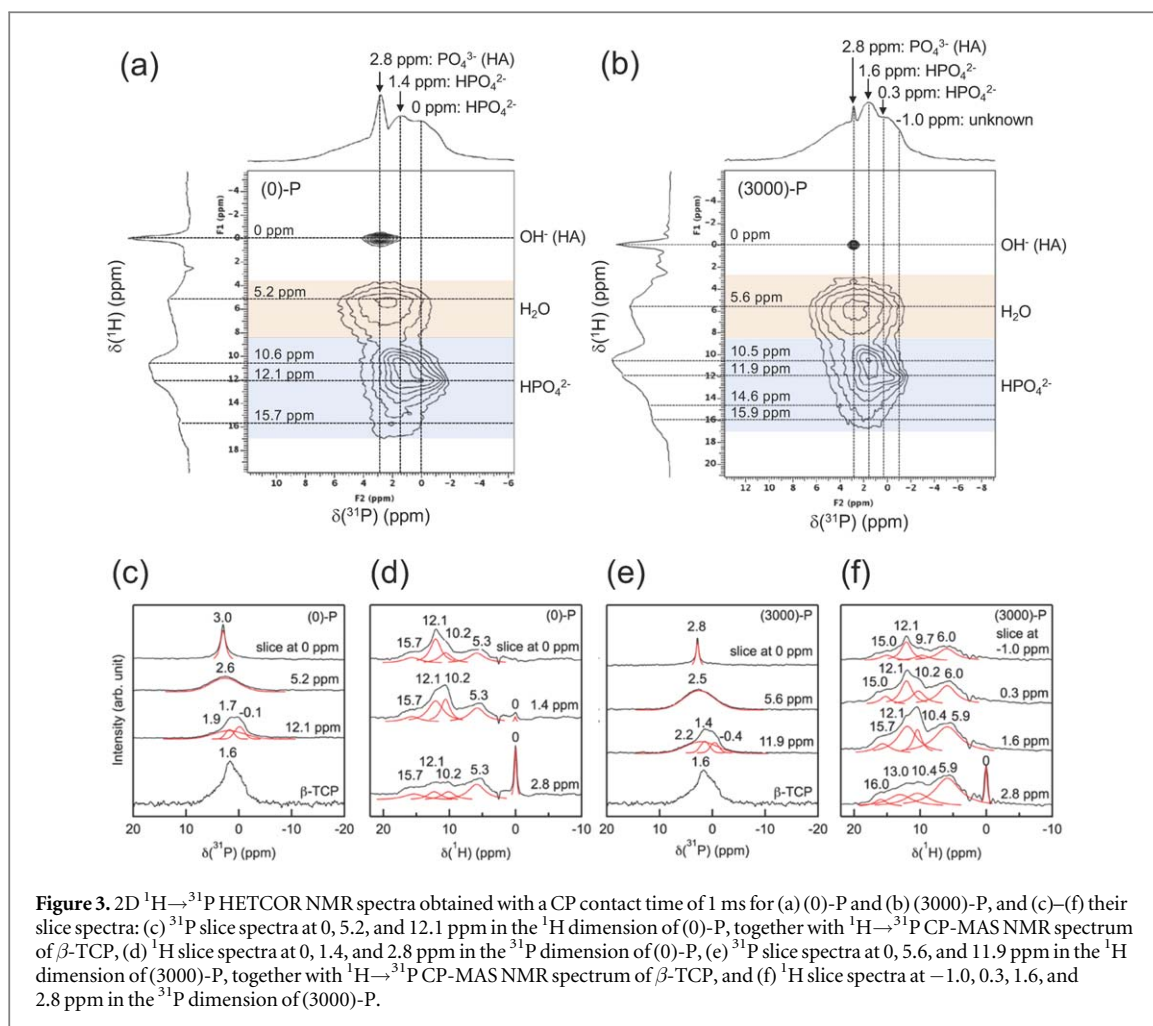


Figure 3. 2D $^1\text{H} \rightarrow ^{31}\text{P}$ HETCOR NMR spectra obtained with a CP contact time of 1 ms for (a) (0)-P and (b) (3000)-P, and (c)–(f) their slice spectra: (c) ^{31}P slice spectra at 0, 5.2, and 12.1 ppm in the ^1H dimension of (0)-P, together with $^1\text{H} \rightarrow ^{31}\text{P}$ CP-MAS NMR spectrum of β -TCP, (d) ^1H slice spectra at 0, 1.4, and 2.8 ppm in the ^{31}P dimension of (0)-P, (e) ^{31}P slice spectra at 0, 5.6, and 11.9 ppm in the ^1H dimension of (3000)-P, together with $^1\text{H} \rightarrow ^{31}\text{P}$ CP-MAS NMR spectrum of β -TCP, and (f) ^1H slice spectra at -1.0 , 0.3 , 1.6 , and 2.8 ppm in the ^{31}P dimension of (3000)-P.

Figure 4 shows the 2D $^1\text{H} \rightarrow ^{31}\text{P}$ HETCOR NMR spectra for (a) (0)-C and (b) (3000)-C. The slice spectrum peak of (0)-C taken at 0 ppm in the ^1H dimension, which was attributed to the protons of OH^- ions in the HA lattice [9], correlated with ^{31}P peak at 3.0 ppm attributed to PO_4^{3-} ions in HA lattice [10] (figure 4(c)). The ^1H peak at 5.4 ppm was assignable to the protons of adsorbed H_2O molecules [9]. This ^1H peak (5.4 ppm) correlated with ^{31}P peaks at 2.1 ppm (unassignable) and at 3.0 ppm corresponding to PO_4^{3-} ions in HA lattice [10], indicating that amorphous hydrated layer was presented on the HA surface. The ^1H peak at 7.9 ppm which was attributed to the protons of HPO_4^{2-} [9] had a correlation with ^{31}P peak at 6.3 ppm corresponding to HPO_4^{2-} of Na_2HPO_4 , which was used as the mixing solution [10]. The ^1H peak at 10.2 ppm allocated to the acidic protons of HPO_4^{2-} in DCPD [9] correlated with ^{31}P peaks at 2.3 ppm (unassignable), at 2.8 ppm attributed to PO_4^{3-} ions in HA lattice [10], and at 6.1 ppm corresponding to HPO_4^{2-} of Na_2HPO_4 [10].

The slice spectrum of figure 4(a) taken at 0 ppm in ^{31}P dimension was assigned to HPO_4^{2-} ion in OCP [11] (figure 4(d)). This ^{31}P peak (0 ppm) had correlations with the ^1H peaks at 0 ppm that was assignable to the protons of OH^- ions in the HA lattice [9] and at 5.4 ppm that was assignable to the protons of adsorbed H_2O molecules [9]. Each ^{31}P peak at 1.7 ppm and 2.9 ppm was assignable to HPO_4^{2-} ion in DCPD [10] and PO_4^{3-} ions in the HA lattice [10], respectively. These ^{31}P peaks correlated with the ^1H peaks at 0 ppm, which was attributed to the protons of OH^- ions in the HA lattice [9], at 5.3 ppm corresponding to protons of adsorbed H_2O molecules [9], and at 8.4 ppm corresponding to the protons of HPO_4^{2-} ions [9]. In addition, the correlation of ^{31}P peak at 2.9 ppm with the ^1H peak at 0 ppm was observed more strongly as compared to 1.7 ppm.

The slice spectra of (3000)-C in both ^1H and ^{31}P dimensions had the same correlations at almost the same positions as compared to (0)-C (figures 4(e) and (f)). However, a difference was observed with the slice spectra taken at 0 and 1.7 ppm in ^{31}P dimension (figure 4(f)), which were assignable to HPO_4^{2-} ion in OCP and DCPD [11], correlated with the ^1H peaks at 11.6 and 12.0 ppm allocated to the protons of HPO_4^{2-} ions [9].

The $^1\text{H} \rightarrow ^{31}\text{P}$ HETCOR NMR spectra of (0)-P and (3000)-P demonstrated more correlation with HPO_4^{2-} ions in DCPD or OCP corresponding to the amorphous hydrated layer on β -TCP surface, whereas no corresponding peak in XRD patterns was observed in figure 1(a). On the other hand, the $^1\text{H} \rightarrow ^{31}\text{P}$ correlation peaks corresponding to HA phase and the amorphous hydrated layer on the HA surface were observed in

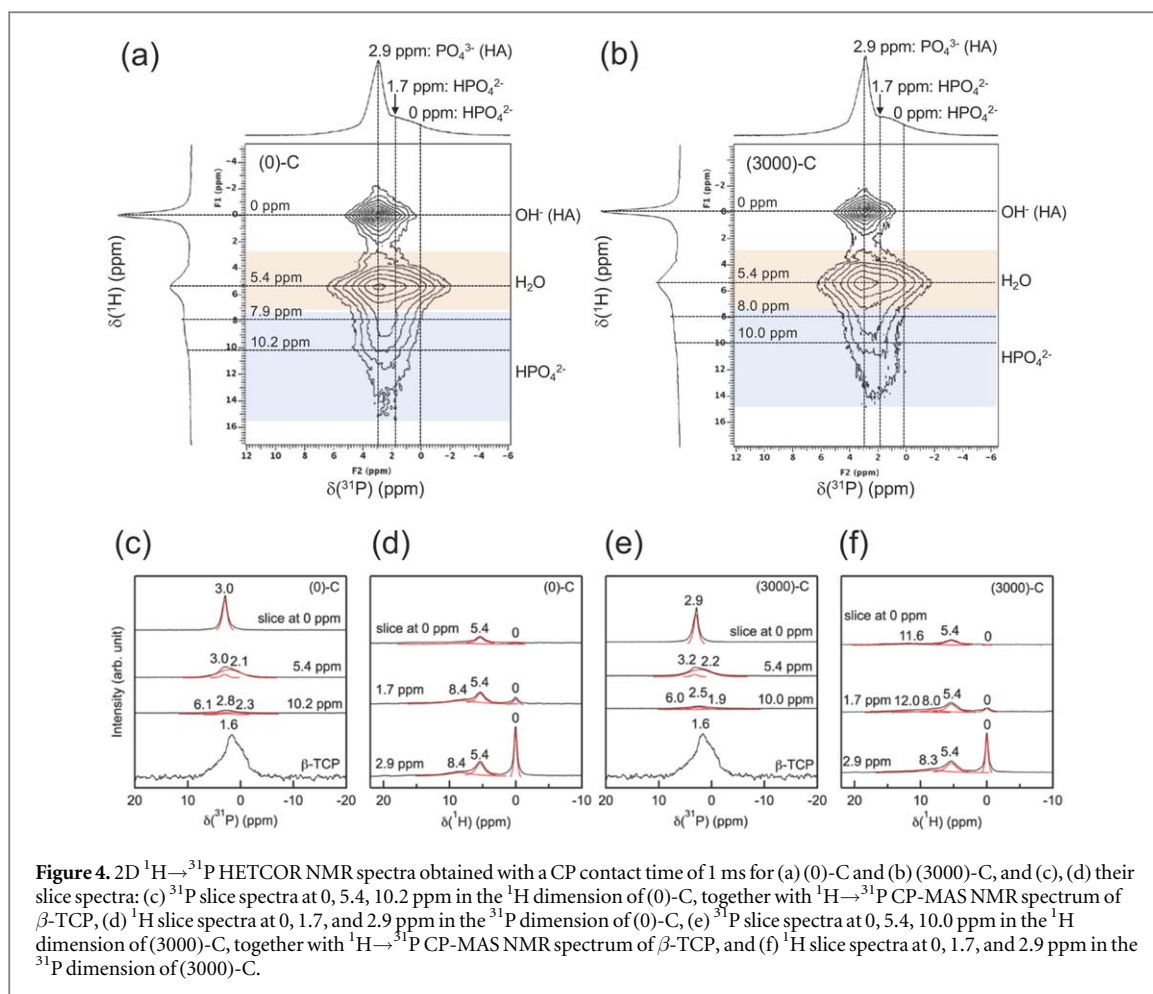


Figure 4. 2D $^1\text{H} \rightarrow ^{31}\text{P}$ HETCOR NMR spectra obtained with a CP contact time of 1 ms for (a) (0)-C and (b) (3000)-C, and (c), (d) their slice spectra: (c) ^{31}P slice spectra at 0, 5.4, 10.2 ppm in the ^1H dimension of (0)-C, together with $^1\text{H} \rightarrow ^{31}\text{P}$ CP-MAS NMR spectrum of β -TCP, (d) ^1H slice spectra at 0, 1.7, and 2.9 ppm in the ^{31}P dimension of (0)-C, (e) ^{31}P slice spectra at 0, 5.4, 10.0 ppm in the ^1H dimension of (3000)-C, together with $^1\text{H} \rightarrow ^{31}\text{P}$ CP-MAS NMR spectrum of β -TCP, and (f) ^1H slice spectra at 0, 1.7, and 2.9 ppm in the ^{31}P dimension of (3000)-C.

figures 4(d) and (f). However, those peaks allocated to the amorphous hydrated layer on β -TCP surface mostly disappeared, suggesting that the amorphous hydrated layer on the β -TCP surface mostly converted to HA during the setting reaction of cement.

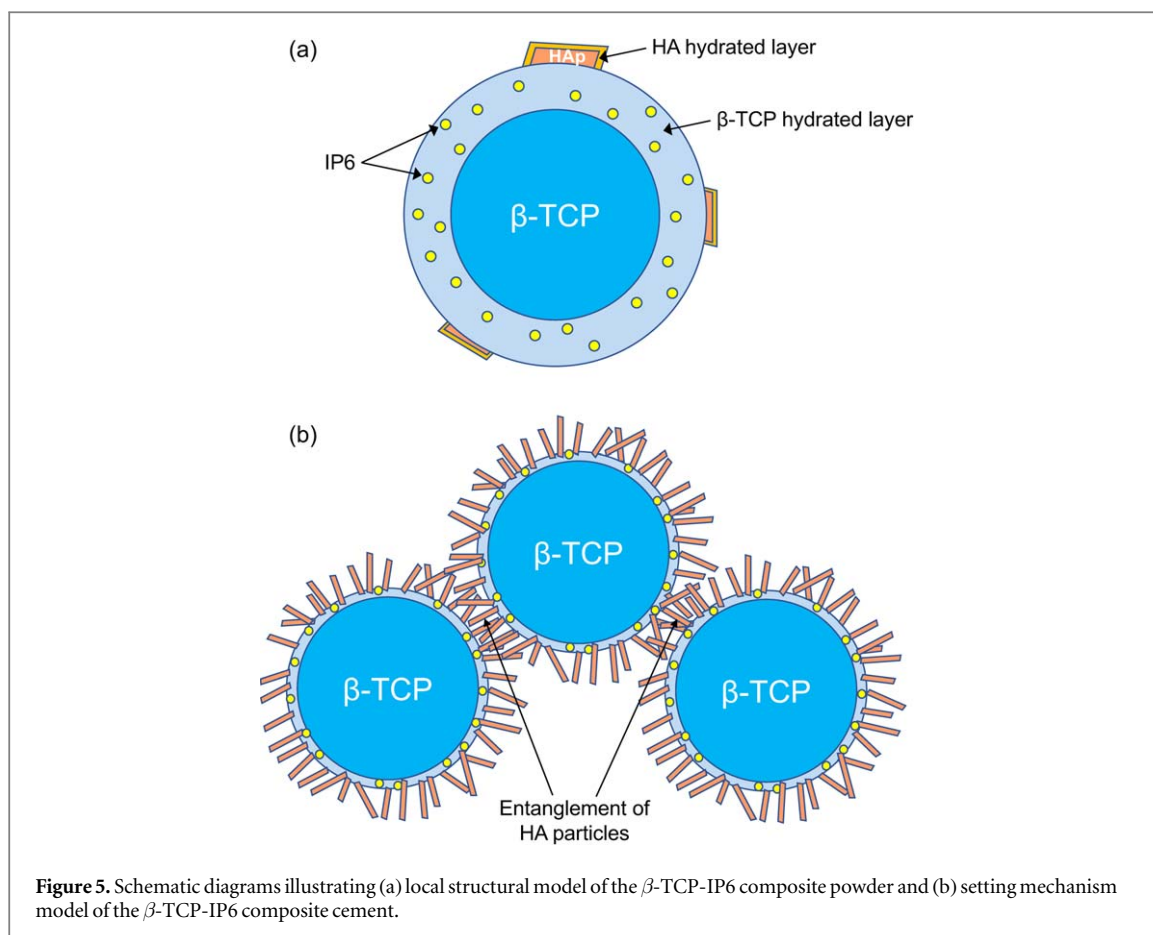
A previous report by Gaffet and Harmelin [12] revealed that ball-milling process induced phase transformation from the crystalline to the amorphous state of silicon powder. Gbrureck *et al* [13] demonstrated that β -TCP ground by ball-milling triggered amorphous fraction within the materials and could be hydrolysed to calcium deficient HA (CDHA) during the setting reaction of cement. However, only the XRD data were provided to show the amorphous fraction. In the present study, 2D $^1\text{H} \rightarrow ^{31}\text{P}$ HETCOR NMR spectra in figures 3 and 4 indicated evidently that the amorphous hydrated layer on the β -TCP surface was formed by the ball-milling process.

It was known that β -TCP could hydrolyze to CDHA by equation (1). However, its hydrolysis was too slow. Goto *et al* [14] reported complete hydrolysis of β -TCP to CDHA was only achieved after 72 h in ammonium solution under hydrothermal process at 120 °C. Indeed, when β -TCP-100 powder was mixed with 2.5 mass% of Na_2HPO_4 at $P/L=1/0.7$ and kept at 100% relative humidity, the β -TCP-100 cement did not convert to HA within 30 d (figure S2). In addition, (0)-P and (3000)-P, which were kept at 37 °C at 100% relative humidity did not convert to HA within 1 month, whereas (0)-P converted to HA significantly and (3000)-P converted to HA after 1 month (figure S3). The results suggested that the amorphous hydrated layer on the (0)-P and (3000)-P surface reacted with water and subsequently converted to HA. (3000)-P took a longer period as it was less reactive than (0)-P due to inclusion of the IP6



Considering the above results, the cement setting reaction were mainly attributed to the amorphous hydrated layer on the β -TCP surface rather than the remaining β -TCP phase in (0)-P and (3000)-P. Nevertheless, it was considered that some of the remaining β -TCP phase in (0)-P and (3000)-P was converted to HA as the remaining β -TCP phase of (0)-C and (3000)-C was less than (0)-P and (3000)-P.

The higher ratio of HA (2 1 1) and β -TCP (0 2 10) for (0)-C (1.10) as compared to (3000)-C (0.45) suggested that the conversion ratio of (3000)-C from β -TCP to HA was lower than (0)-C (table 1). Figure 2(b) also demonstrated



that the conversion of (3000)-P from β -TCP to HA during ball-milling was lesser than (0)-P. Grases *et al* [15] reported that HA crystallization was prevented in the presence of phytate in synthetic urine solution. In addition, it was recently reported by Meininger *et al* [16] that phytic acid was favorable as a setting retardant of a brushite cement, as phytic acid retarded the crystallization of DCP. Hence, it was considered that the IP6 in (3000)-P composite powder might inhibit the conversion of β -TCP to HA, and resulting in more β -TCP phase remained in (3000)-C than (0)-C.

Based on the above results, schematic diagrams of (a) local structural model of the β -TCP-IP6 composite powder and (b) setting mechanism model of the β -TCP-IP6 composite cement are illustrated in figure 5. An amorphous hydrated layer, along with small amount of HA was formed on the surface of β -TCP during the ball-milling process (figure 5(a)). The IP6 in the hydrated layer on β -TCP surface was suggested to inhibit the formation of HA. The structure of the (0)-P without IP6 was almost identical to (3000)-P but had a different ratio of the HA phase and hydrated layer. When the β -TCP-IP6 composite powder was added to the mixing solution, the hydrated layer of β -TCP was mostly converted to HA, with some β -TCP phase remained. Thereafter, this was followed by an inter-entanglement between the HA crystals on the β -TCP-IP6 cement (figure 5(b)). This setting mechanism of the cement, i.e. dissolution and precipitation processes, was similar to the conventional CPC with a slight discrepancy. The setting reaction of the conventional CPC began with the dissolution of crystalline material(s), followed by the precipitation of final product. On the other hand, in this cement, the dissolution of the hydrated layer on β -TCP surface and subsequent precipitation of HA were mainly involved during the cement setting reaction. In addition, it was expected that the unreacted β -TCP particles in (3000)-C (figure S1(a)) would be gradually resorbed in human body and eventually get replaced by the host bones.

Overall, the present study demonstrated that NMR analysis of local chemical structure of powder and its cement was beneficial in understanding how both the crystalline and non-crystalline phase were involved during the setting reaction of cement. As such, this method could also be applicable for understanding the setting mechanism of the conventional cement such as DCPD—tetracalcium phosphate cement or β -TCP—monocalcium phosphate monohydrate cement.

4. Conclusions

The present study investigated the setting mechanism of the CPC, which was fabricated using β -TCP-IP6 composite powder. The effect of IP6 on the local chemical structure of the β -TCP-IP6 composite powder and its hardened cement was examined using solid-state NMR spectroscopy. The $^1\text{H} \rightarrow ^{31}\text{P}$ HETCOR NMR spectrum revealed that an amorphous hydrated layer, along with small amount of HA was formed on the surface of β -TCP during the ball-milling process. As a higher amount of β -TCP phase was remained in (3000)-C than (0)-C, this suggested that the IP6 in the hydrated layer might have inhibited the HA formation. The results showed that the setting reaction of the cements was triggered by the dissolution of the amorphous hydrated layer on β -TCP surface and subsequent precipitation, followed by the inter-entanglement between the HA crystals on the β -TCP.

Acknowledgments

The authors thank to Prof S Hayakawa and Assoc. Prof T Yoshioka for their experimental assistance and guidance.

ORCID iDs

Toshiisa Konishi  <https://orcid.org/0000-0002-6422-8157>

Poon Nian Lim  <https://orcid.org/0000-0003-4693-4688>

References

- [1] Bohner M 2007 Reactivity of calcium phosphate cements *J. Mater. Chem.* **17** 3980
- [2] Konishi T, Takahashi S, Zhuang Z, Nagata K, Mizumoto M, Honda M, Takeuchi Y, Matsunari H, Nagashima H and Aizawa M 2013 Biodegradable β -tricalcium phosphate cement with anti-washout property based on chelate-setting mechanism of inositol phosphate *J. Mater. Sci. Mater. Med.* **24** 1383–94
- [3] Boudeville P, Serraj S, Leloup J M, Margerit J, Pauvert B and Terol A 1999 Physical properties and self-setting mechanism of calcium phosphate cements from calcium bis-dihydrogenophosphate monohydrate and calcium oxide *J. Mater. Sci. Mater. Med.* **10** 99–109
- [4] Legrand A P, Sfihi H, Lequeux N and Lemaitre J 2009 ^{31}P solid-state NMR study of the chemical setting process of a dual-paste injectable brushite cements *J. Biomed. Mater. Res. B* **91** 46–54
- [5] Fowler B O, Moreno E C and Brown W E 1966 Infra-red spectra of hydroxyapatite, octacalcium phosphate and pyrolysed octacalcium phosphate *Arch. Oral Biol.* **11** 477–92
- [6] He Z, Honeycutt C W, Zhang T and Bertsch P M 2006 Preparation and FT-IR characterization of metal phytate compounds *J. Environ. Qual.* **35** 1319
- [7] Ganesan K and Epple M 2008 Calcium phosphate nanoparticles as nuclei for the preparation of colloidal calcium phytate *New J. Chem.* **32** 1326–30
- [8] Jäger C, Welzel T, Meyer-Zaika W and Epple M 2006 A solid-state NMR investigation of the structure of nanocrystalline hydroxyapatite *Magn. Reson. Chem.* **44** 573–80
- [9] Yesinowski J P and Eckert H 1987 Hydrogen environments in calcium phosphates: H MAS NMR at high spinning speeds *J. Am. Chem. Soc.* **109** 6274–82
- [10] Rothwell W P, Waugh J S and Yesinowski J P 1980 High-resolution variable-temperature ^{31}P NMR of solid calcium phosphates *J. Am. Chem. Soc.* **102** 2637–43
- [11] Davies E, Duer M J, Ashbrook S E and Griffin J M 2012 Applications of NMR crystallography to problems in biomineralization: refinement of the crystal structure and ^{31}P solid-state NMR spectral assignment of octacalcium phosphate *J. Am. Chem. Soc.* **134** 12508–15
- [12] Gaffet E and Harmelin M 1990 Crystal-amorphous phase transition induced by ball-milling in silicon *J. Less-Common Met.* **157** 201–22
- [13] Gbureck U, Grolms O, Barralet J E, Grover L M and Thull R 2003 Mechanical activation and cement formation of β -tricalcium phosphate *Biomaterials* **24** 4123–31
- [14] Goto T, Kim I Y, Kikuta K and Ohtsuki C 2012 Comparative study of hydroxyapatite formation from α - and β -tricalcium phosphates under hydrothermal conditions *J. Ceram. Soc. Japan* **120** 131–7
- [15] Grases F, Ramis M and Costa-Bauzá A 2000 Effects of phytate and pyrophosphate on brushite and hydroxyapatite crystallization. Comparison with the action of other polyphosphates *Urol. Res.* **28** 136–40
- [16] Meininger S, Blum C, Schamel M, Barralet J E, Ignatius A and Gbureck U 2017 Phytic acid as alternative setting retarder enhanced biological performance of dicalcium phosphate cement *in vitro Sci. Rep.* **7** 558